# Cumulative two-pulse photon echoes

A. Schenzle,* R. G. DeVoe, and R. G. Brewer
*IBM Research Laboratory, San Jose, California 95193*
(Received 25 April 1984)

This paper reports an unusual photon-echo phenomenon where a train of echoes, generated by a repeating two-pulse sequence, exhibits growth rather than damping. The effect, which is observed in the impurity-ion crystal $Pr^{3+}$:$YAlO_3$, results from an electronic ground-state population grating that is created by the two-pulse sequence and is stored coherently as a modulation in the frequency domain. The depth of modulation increases with increasing $n$, where $n$ is the number of the two-pulse sequence—a result which is predicted in a three-level density-matrix theory. The effect is closely related to previous stimulated or three-pulse photon echoes but differs in that growth is observed directly for the first time in the simpler two-pulse sequence.

## I. INTRODUCTION

Following the initial work of Carr and Purcell,[1] a number of multipulse spin-[2–5] and photon-echo[6–8] experiments have been reported. In liquids, the technique has allowed measurement of the spatial diffusion of spins which are dominated either by inhomogeneous static[1,3] or radio-frequency (rf)[2] magnetic fields. In solids, with more elaborate rf multipulse sequences,[4,5] spin dipolar line broadening has been reduced dramatically. In gases, the optical analog of the Carr-Purcell method has permitted the detection of long-range velocity-changing collisions,[6] and more recently, a train of stimulated three-pulse photon echoes has been used to monitor optical dephasing times in solids on a picosecond time scale.[7]

In this paper, we report that photon echoes generated by a repetitive two-pulse sequence (Fig. 1) can actually exhibit growth, contrary to intuition and past experience where the echo envelope invariably damps. This growth phenomenon is displayed clearly in Fig. 2 for the case of the impurity ion crystal $Pr^{3+}$:$YAlO_3$ at 1.6 K where the echo amplitude increases linearly with time. Since the interval $T$ between neighboring pulse sequences is much greater than the optical dephasing time $T_2$, the only possibility for a *memory* effect which leads to echo growth resides in the optically excited population distribution. The physical origin of this effect arises from a population distribution or grating of the form

$$w \sim a\cos(\Delta\tau)+b\sin(\Delta\tau) \tag{1.1}$$

that is modulated in the frequency domain $\Delta$ due to a two-pulse delay time $\tau$. Successive two-pulse sequences increase the depth of modulation, the coefficients $a$ and $b$, where (1.1) contains the required Fourier components for two-pulse echo formation leading to echo growth. A population memory effect also arises in the three-pulse stimulated photon echo, either in a single[9,10] or multipulse[7] sequence, although past observations have not revealed the growth pattern directly in contrast to Fig. 2.

We show here that a two-pulse echo growth pattern can be explained in principle using a two-level quantum system as a model. However, the numerical values of the decay parameters and the conditions of our experiment argue in favor of a three-level model where the population is stored in a bottleneck or third level. The bulk of the paper is concerned with these two calculations.

Finally, we note that since the optical homogeneous linewidth $Pr^{3+}YAlO_3$ is but a few kilohertz, reproducible echo growth measurements are made possible only through the use of a (gated) ultrastable cw dye laser having a linewidth of 300 Hz or less.

## II. TWO-LEVEL MODEL

We assume that two-level atoms are repetitively excited by the square-wave optical two-pulse sequence of Fig. 1 where $\tau$ is the delay time of the second pulse and $T$ is the repetition time of the two-pulse sequence. We further assume that (1) the laser frequency remains fixed within the

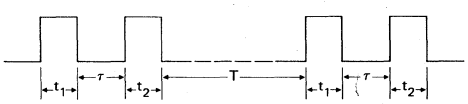


FIG. 1. A repetitive two-pulse echo sequence where $n$ is the number of times the sequence repeats.

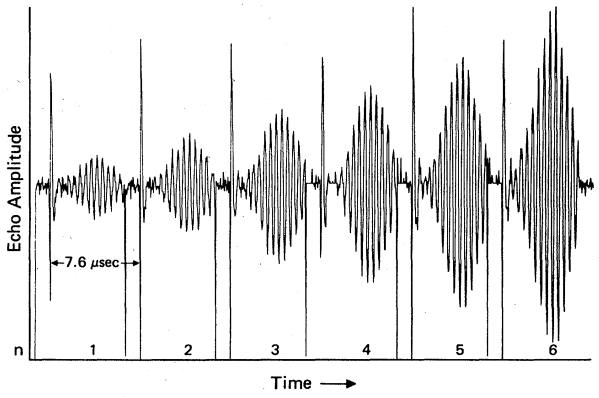


FIG. 2. Cumulative two-pulse photon echoes observed in 0.1 at.% $Pr^{3+}$:$YAlO_3$ at 1.6 K. The echo amplitude grows as the two-pulse sequence $n$ increases.

 

sample's homogeneous width, (2) the optical pulse area $\theta=(\mu_{12}/\hbar)\int_{-\infty}^{\infty}\epsilon(z,t)dt$ is small, satisfying $\theta\ll\pi/2$, and (3) the repetition period is much longer than the optical dephasing time, $T\gg T_2$. Condition (1) guarantees that the same packets within the inhomogeneous line shape are interrogated throughout the pulse train and thus will faithfully generate the desired echo envelope. In Sec. IV, the complication resulting from an unstable laser is discussed. Condition (2) is required if echo growth is to occur. Condition (3) assures that phase memory is retained in the frequency domain rather than in the time domain.

The $2\times2$ density-matrix equations of motion,[11] the Bloch equations,

$$\begin{aligned}\dot{\tilde{\rho}}_{12}&=(i\Delta-1/T_2)\tilde{\rho}_{12}+(i\chi/2)w\ ,\\ \dot{\tilde{\rho}}_{21}&=\dot{\tilde{\rho}}^{*}_{12}\ ,\\ \dot{w}&=-(w-w_0)/T_1-i\chi(\tilde{\rho}_{21}-\tilde{\rho}_{12})\ ,\end{aligned}\tag{2.1}$$

are to be solved during pulse excitation and between pulses with the added complication that the pulse sequence is repetitive. Here, the tilde signifies the optical rotating frame, the population difference of levels 2 and 1 is defined by $w=\rho_{22}-\rho_{11}$, the Rabi frequency is $\chi=\mu_{12}E_0/\hbar$, and the tuning parameter $\Delta=\omega_{21}-\Omega$, where $\mu_{12}$ is the optical transition matrix element, $E_0$ the optical field amplitude, $\omega_{21}$ the energy level splitting, and $\Omega$ the optical frequency.

The pulses are assumed to be sufficiently short that damping can be neglected and $\Delta=0$. On the other hand, if $\Delta$ is retained, the simplicity of the treatment given below vanishes. For the initial condition

$$[\tilde{\rho}_{12}(0),\tilde{\rho}_{21}(0),w(0)]\tag{2.2}$$

at time $t=0$, the pulse solutions of (2.1) are

$$\begin{aligned}\tilde{\rho}_{12}(t)&=\tfrac{1}{2}\tilde{\rho}_{12}(0)[1+\cos(\chi t)]\\ &\quad+\tfrac{1}{2}\tilde{\rho}_{21}(0)[1-\cos(\chi t)]+\tfrac{1}{2}iw(0)\sin(\chi t)\ ,\\ \tilde{\rho}_{2}&\qquad 1-\cos(\chi t)]\\ &\quad+\tfrac{1}{2}\tilde{\rho}_{21}(0)[1+\cos(\chi t)]-\tfrac{1}{2}iw(0)\sin(\chi t),\\ w(t)&=i\tilde{\rho}_{12}(0)\sin(\chi t)-i\tilde{\rho}_{21}(0)\sin(\chi t)+w(0)\cos(\chi t)\ .\end{aligned}\tag{2.3}$$

Between pulses, $\chi=0$ and (2.1) yields

$$\begin{aligned}\tilde{\rho}_{21}(t)&=\tilde{\rho}_{12}(0)e^{(i\Delta-1/T_2)t}\ ,\\ \tilde{\rho}_{21}(t)&=\tilde{\rho}_{21}(0)e^{-(i\Delta+1/T_2)t}\ ,\\ w(t)&=w(0)e^{-t/T_1}+w_0(1-e^{-t/T_1})\ .\end{aligned}\tag{2.4}$$

We now cast the problem in matrix form, writing the state vector as

$$\underline{X}(t)=\begin{bmatrix}\tilde{\rho}_{12}(t)\\ \tilde{\rho}_{21}(t)\\ w(t)\\ w_0\end{bmatrix}\ .\tag{2.5}$$

A time evolution matrix $\underline{\Pi}(t)$ then transforms an initial value $\underline{X}_j(0)$, the $j$th component of the state vector, into the $i$th component

$$X_i(t)=\Pi_{ij}(t)X_j(0)\tag{2.6}$$

at the later time $t$. From (2.3) and $w_0=1$, the $\underline{\Pi}$ matrix during a pulse is

$$\underline{F}(t)=\begin{bmatrix}\frac{1}{2}[1+\cos(\chi t)] & \frac{1}{2}[1-\cos(\chi t)] & \frac{1}{2}i\sin(\chi t) & 0\\ \frac{1}{2}[1-\cos(\chi t)] & \frac{1}{2}[1+\cos(\chi t)] & -\frac{1}{2}i\sin(\chi t) & 0\\ i\sin(\chi t) & -i\sin(\chi t) & \cos(\chi t) & 0\\ 0 & 0 & 0 & 1\end{bmatrix}\ .\tag{2.7}$$

The $\underline{\Pi}$ matrix between pulses follows from (2.4) and is given by

$$\underline{D}(t)=\begin{bmatrix}e^{(i\Delta-1/T_2)t} & 0 & 0 & 0\\ 0 & e^{-(i\Delta+1/T_2)t} & 0 & 0\\ 0 & 0 & e^{-t/T_1} & (1-e^{-t/T_1})\\ 0 & 0 & 0 & 1\end{bmatrix}\ .\tag{2.8}$$

Successive application of (2.7) and (2.8) for the two-pulse sequence of Fig. 1 generates the echo operator

$$\underline{E}(t)=\underline{D}(t)\underline{F}(t_2)\underline{D}(\tau)\underline{F}(t_1)\ ,\tag{2.9}$$

where $t$ is the time interval measured from the end of the second pulse, $t_1$ and $t_2$ are the first and second pulse widths, and $\tau$ is the second pulse delay time.

For the $n$-pulse sequence of Fig. 1, repeated application of (2.9) results in

$$\underline{X}(t)=\underline{E}(t)[\underline{E}(T)]^{n-1}\underline{X}(0)\ ,\tag{2.10}$$

where the initial condition

$$\underline{X}(0)=w_0\begin{bmatrix}0\\0\\1\\1\end{bmatrix}\ .\tag{2.11}$$

Here, the time dependence of the element $\underline{X}(t)$ appears only in $E(t)$ corresponding to the $n$th or last two-pulse sequence.

The echo matrix $\underline{E}(T)$ simplifies considerably with the assumption $T\gg T_2$, allowing us to ignore the damping terms $e^{-T/T_2}$. For a single sequence, detailed evaluation of (2.9) gives

$$\underline{E}(T)=\begin{bmatrix}0 & 0 & 0 & 0\\ 0 & 0 & 0 & 0\\ E_{31} & E_{32} & E_{33} & E_{34}\\ 0 & 0 & 0 & 1\end{bmatrix}\ ,\tag{2.12}$$

while for $n$ sequences

$$[\underline{E}(T)]^n=\begin{bmatrix} 0 & 0 & 0 & 0 \\ 0 & 0 & 0 & 0 \\ E_{33}^{n-1}E_{31} & E_{33}^{n-1}E_{32} & E_{33}^{n} & E_{34}\sum_{l=0}^{n-1}E_{33}^{l} \\ 0 & 0 & 0 & 1 \end{bmatrix} . \tag{2.13}$$

The echo signal for an $n$-pulse sequence is essentially given by the polarization or off-diagonal element

$$[\tilde{\rho}_{12}(t)]_n=E_{1j}(t)[\underline{E}(T)]_{jl}^{n}{}^{-1}X_l(0) \tag{2.14}$$

$$=E_{13}(t)\left[E_{33}^{n-1}+E_{34}\sum_{l=0}^{n-2}E_{33}^{l}\right]W_0 , \tag{2.15}$$

where (2.14) follows from (2.10), the initial condition $X_l(0)$ is given by (2.11), and matrix multiplication of (2.11) and (2.13) produces (2.15). Here,

$$E_{13}(t)=\tfrac{1}{2}ie^{(i\Delta-1/T_2)t}\{\tfrac{1}{2}[1+\cos(\chi t_2)]\sin(\chi t_1)e^{(i\Delta-1/T_2)\tau} -\tfrac{1}{2}[1-\cos(\chi t_2)]\sin(\chi t_1)e^{-(i\Delta+1/T_2)\tau}+\cos(\chi t_1)\sin(\chi t_2)e^{-\tau/T_1}\} , \tag{2.16}$$

$$E_{33}(T)=e^{-T/T_1}[\cos(\chi t_2)\cos(\chi t_1)e^{-\tau/T_1}-\tfrac{1}{2}\sin(\chi t_2)\sin(\chi t_1)e^{-(i\Delta+1/T_2)\tau}-\tfrac{1}{2}\sin(\chi t_2)\sin(\chi t_1)e^{(i\Delta-1/T_2)\tau}] , \tag{2.17}$$

$$E_{34}(T)=\cos(\chi t_2)e^{-T/T_1}(1-e^{-\tau/T_1})+(1-e^{-T/T_1}) . \tag{2.18}$$

Equation (2.15) is to be averaged over the inhomogeneous line shape, but this procedure does not alter the results to be discussed and will be ignored.

Inspection of (2.17) and (2.18) reveals that in the limit $T/T_1\to\infty$, $\sum_{l=0}^{n-2}E_{33}^{l}(T)=1$, $E_{34}(T)=1$, and consequently

$$[\tilde{\rho}_{12}(t)]_n=E_{13}(t) . \tag{2.19}$$

That is to say that the population grating or memory is erased for times longer than the population decay time $T_1$ and the echo signal (2.19) has its origin only in the last pulse sequence $E_{13}(t)$. For the experiment of Fig. 2, $T/T_1\sim 2$ and here numerical evaluation of (2.15) shows that $\tilde{\rho}_{12}(t)_n$ is essentially given by (2.19). This model, therefore, is in disagreement with the observations, making it clear that a population bottleneck is needed so that the population grating is not filled in. In Sec. III, a three-level model satisfies this requirement.

To complete this section, we next consider the other extreme when $T/T_1\ll 1$ and assume that small area pulses are applied where

$$\theta_1=\chi t_1\ll\pi/2,\quad \theta_2=\chi t_2\ll\pi/2 . \tag{2.20}$$

We then have

$$E_{13}(t)=\tfrac{1}{2}ie^{(i\Delta-1/T_2)t}[\theta_1 e^{(i\Delta-1/T_2)t} -\tfrac{1}{4}\theta_1\theta_2^2 e^{-(i\Delta+1/T_2)\tau}+\theta_2] , \tag{2.21}$$

$$[E_{33}(T)]^{n-1}=[1-\tfrac{1}{2}\theta_1\theta_2 e^{-\tau/T_2}(e^{i\Delta\tau}+e^{-i\Delta\tau})]^{n-1} \sim[1-\tfrac{1}{2}(n-1)\theta_1\theta_2 e^{-\tau/T_2}(e^{i\Delta\tau}+e^{-i\Delta\tau})] , \tag{2.22}$$

$$E_{34}(T)\sim 0 , \tag{2.23}$$

where (2.22) is readily expanded in $(n-1)$ because of the smallness of $\theta_1\theta_2$. The echo signal derived from (2.15) now takes the form

$$[\tilde{\rho}_{12}(t)]_n=\tfrac{1}{8}(2n-1)i\theta_1\theta_2^2 e^{i\Delta(t-\tau)}e^{-(t+\tau)/T_2} , \tag{2.24}$$

where only the echo rephasing terms are retained. In contrast to (2.19), the echo amplitude increases linearly as $2n-1=1,3,5,\ldots$ as the pulse sequence number $n$ increases.

## III. THREE-LEVEL MODEL

The density-matrix equations of motion for the two-level problem (2.1) are extended by adding level 3 as in Fig. 3 which allows the population transfer $2\to 3$ at the rate $\gamma_2$, $3\to 1$ ($\gamma_3$) as well as $2\to 1$ ($\gamma_1$). The reverse processes are considered improbable and are ignored. We then have

$$\begin{aligned} \dot{\tilde{\rho}}_{12}&=(i\Delta-1/T_2)\tilde{\rho}_{12}+\tfrac{1}{2}i\chi(\rho_{22}-\rho_{11}) , \\ \dot{\tilde{\rho}}_{21}&=\dot{\tilde{\rho}}_{12}^{*} , \\ \dot{\rho}_{11}&=\tfrac{1}{2}i\chi(\tilde{\rho}_{21}-\tilde{\rho}_{12})+\gamma_1\rho_{22}+\gamma_3\rho_{33} , \\ \dot{\rho}_{22}&=-\tfrac{1}{2}i\chi(\tilde{\rho}_{21}-\tilde{\rho}_{12})-\gamma_0\rho_{22} , \end{aligned} \tag{3.1}$$

where

$$\gamma_0=\gamma_1+\gamma_2$$

and population is conserved among the three states satisfying

$$\rho_{11}+\rho_{22}+\rho_{33}=1 . \tag{3.2}$$

For a significant population bottleneck, we assume that

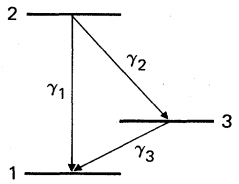


FIG. 3. Population decay rates $\gamma_i$ ($i=1,2,3$) are indicated for the three-level model where level 3 is the bottleneck.

$$\gamma_2 \gg \gamma_1, \gamma_3 \,. \tag{3.3}$$

During pulse excitation, we again neglect $\Delta$ and damping so that the two-level solutions (2.3) apply but with the additional condition

$$\rho_{22}(t)+\rho_{11}(t)=\rho_{22}(0)+\rho_{11}(0) \,. \tag{3.4}$$

We obtain for pulse excitation

$$\begin{aligned}
\tilde{\rho}_{12}(t)&=\tfrac{1}{2}\tilde{\rho}_{12}(0)[1+\cos(\chi t)]+\tfrac{1}{2}\tilde{\rho}_{21}(0)[1-\cos(\chi t)] \\
&\quad -\tfrac{1}{2}i\rho_{11}(0)\sin(\chi t)+\tfrac{1}{2}i\rho_{22}(0)\sin(\chi t) \,, \\
\tilde{\rho}_{21}(t)&=\tilde{\rho}_{12}(t)^* \,, \\
\rho_{11}(t)&=-\tfrac{1}{2}i\tilde{\rho}_{12}(0)\sin(\chi t)+\tfrac{1}{2}i\tilde{\rho}_{21}(0)\sin(\chi t) \\
&\quad +\tfrac{1}{2}\rho_{11}(0)[1+\cos(\chi t)]+\tfrac{1}{2}\rho_{22}(0)[1-\cos(\chi t)] \,, \\
\rho_{22}(t)&=\tfrac{1}{2}i\tilde{\rho}_{12}(0)\sin(\chi t)-\tfrac{1}{2}i\tilde{\rho}_{21}(0)\sin(\chi t) \\
&\quad +\tfrac{1}{2}\rho_{11}(0)[1-\cos(\chi t)]+\tfrac{1}{2}\rho_{22}(0)[1+\cos(\chi t)] \,.
\end{aligned} \tag{3.5}$$

The solutions between pulses are found from (3.1) with $\chi=0$,

$$\begin{aligned}
\tilde{\rho}_{12}(t)&=\tilde{\rho}_{12}(0)e^{(i\Delta-1/T_2)t} \,, \\
\rho_{21}(t)&=\tilde{\rho}_{12}(t)^* \,, \\
\rho_{11}(t)&=\rho_{11}(0)e^{-\gamma_3 t}+\rho_{22}(0)\lambda(e^{-\gamma_3 t}-e^{-\gamma_0 t}) \\
&\quad +(1-e^{-\gamma_3 t}) \,, \\
\rho_{22}(t)&=\rho_{22}(0)e^{-\gamma_0 t} \,,
\end{aligned} \tag{3.6}$$

where

$$\lambda=(\gamma_3-\gamma_1)/(\gamma_3-\gamma_0) \,,$$

$$\gamma_0=\gamma_1+\gamma_2 \,,$$

and small terms have been dropped through the inequality (3.3).

Proceeding as in the two-level model, we define a state vector

$$\underline{X}(t)=\begin{bmatrix} \tilde{\rho}_{12}(t) \\ \tilde{\rho}_{21}(t) \\ \rho_{11}(t) \\ \rho_{22}(t) \\ 1 \end{bmatrix} \,. \tag{3.7}$$

The time-evolution matrix during a pulse

$$\underline{F}(t)=\begin{bmatrix} \tfrac{1}{2}[1+\cos(\chi t)] & \tfrac{1}{2}[1-\cos(\chi t)] & -\tfrac{1}{2}i\sin(\chi t) & \tfrac{1}{2}i\sin(\chi t) & 0 \\ \tfrac{1}{2}[1-\cos(\chi t)] & \tfrac{1}{2}[1+\cos(\chi t)] & \tfrac{1}{2}i\sin(\chi t) & -\tfrac{1}{2}i\sin(\chi t) & 0 \\ -\tfrac{1}{2}i\sin(\chi t) & \tfrac{1}{2}i\sin(\chi t) & \tfrac{1}{2}[1+\cos(\chi t)] & \tfrac{1}{2}[1-\cos(\chi t)] & 0 \\ \tfrac{1}{2}i\sin\chi t & -\tfrac{1}{2}i\sin(\chi t) & \tfrac{1}{2}[1-\cos(\chi t)] & \tfrac{1}{2}[1+\cos(\chi t)] & 0 \\ 0 & 0 & 0 & 0 & 1 \end{bmatrix} \tag{3.8}$$

follows from (3.5). Between pulses, the matrix

$$\underline{D}(t)=\begin{bmatrix} e^{(i\Delta-1/T_2)t} & 0 & 0 & 0 & 0 \\ 0 & e^{-(i\Delta+1/T_2)t} & 0 & 0 & 0 \\ 0 & 0 & e^{-\gamma t} & \lambda(e^{-\gamma_3 t}-e^{-\gamma_0 t}) & (1-e^{-\gamma_3 t}) \\ 0 & 0 & 0 & e^{-\gamma_0 t} & 0 \\ 0 & 0 & 0 & 0 & 1 \end{bmatrix} \tag{3.9}$$

follows from (3.6).

The echo signal for the $n$th pulse sequence now assumes the form

$$[\tilde{\rho}_{12}(t)]_n=E_{1j}(t)[\underline{E}(T)]_{jk}^{n-1}\begin{bmatrix} 0 \\ 0 \\ 1 \\ 0 \\ 1 \end{bmatrix} \,, \tag{3.10}$$

where the column vector specifies the initial condition. The echo matrix $E(T)$, (2.10), is evaluated using the approximations

$$T \gg T_2, \quad |\lambda| \ll 1, \quad \gamma_0 T \gg 1, \quad \gamma_3 T \ll 1 \,, \tag{3.11}$$

where the first inequality was introduced in the two-level model, the second follows from (3.3), the third assumes the de-

cay time of level 2 is rapid compared to the time $T$ between two successive pulse sequences, and the fourth guarantees that the population grating is not erased during the experiment. For a single-pulse sequence, evaluation of the echo matrix (2.9) gives

$$\underline{E}(T)=\begin{bmatrix} 0 & 0 & 0 & 0 & 0 \\ 0 & 0 & 0 & 0 & 0 \\ E_{31} & E_{32} & E_{33} & E_{34} & E_{35} \\ 0 & 0 & 0 & 0 & 0 \\ 0 & 0 & 0 & 0 & 0 \end{bmatrix} . \tag{3.12}$$

For an $n$-pulse sequence

$$\underline{E}^n(T)=\begin{bmatrix} 0 & 0 & 0 & 0 & 0 \\ 0 & 0 & 0 & 0 & 0 \\ E_{33}^{n-1}E_{31} & E_{33}^{n-1}E_{32} & E_{33}^{n} & E_{33}^{n-1}E_{34} & E_{35}\sum_{l=0}^{n-1}E_{33}^{l} \\ 0 & 0 & 0 & 0 & 0 \\ 0 & 0 & 0 & 0 & 0 \end{bmatrix} . \tag{3.13}$$

Since

$$[\underline{E}(T)]^{n-1}\begin{bmatrix}0\\0\\1\\0\\1\end{bmatrix}=\begin{bmatrix} 0 \\ 0 \\ [E_{33}(t)]^{n-1}+E_{35}(T)\sum_{l=0}^{n-2}E_{33}^{l} \\ 0 \\ 1 \end{bmatrix} , \tag{3.14}$$

(3.10) becomes

$$[\tilde{\rho}_{12}(t)]_n=E_{13}(t)\left[[E_{33}(T)]^{n-1}+E_{35}(T)\sum_{l=0}^{n-2}E_{33}^{l}(T)\right] . \tag{3.15}$$

Here, $E_{15}(t)=0$,

$$E_{13}(t)=-\tfrac{1}{4}i\sin(\chi t_1)[1+\cos(\chi t_2)]e^{(i\Delta-1/T_2)(t+\tau)}+\tfrac{1}{4}i\sin(\chi t_1)[1-\cos(\chi t_2)]e^{(i\Delta-1/T_2)t_e-(i\Delta+1/T_2)\tau}$$
$$-\tfrac{1}{4}i\sin(\chi t_2)[1+\cos(\chi t_1)]e^{(i\Delta-1/T_2)t}+\tfrac{1}{4}i\sin(\chi t_2)[1-\cos(\chi t_1)]e^{(i\Delta-1/T_2)t}e^{-\gamma_0\tau} , \tag{3.16}$$

$$E_{33}(T)=e^{-\gamma_3 T}\{-\tfrac{1}{4}\sin(\chi t_1)\sin(\chi t_2)e^{(i\Delta-1/T_2)\tau}-\tfrac{1}{4}\sin(\chi t_1)\sin(\chi t_2)e^{-(i\Delta+1/T_2)\tau}$$
$$+\tfrac{1}{4}[1+\cos(\chi t_1)][1+\cos(\chi t_2)]e^{-\gamma_3\tau}+\tfrac{1}{4}[1-\cos(\chi t_1)][1-\cos(\chi t_2)]e^{-\gamma_0\tau}\} , \tag{3.17}$$

$$E_{35}(T)=\tfrac{1}{2}e^{-\gamma_3 T}[1+\cos(\chi t_2)](1-e^{-\gamma_3\tau})+(1-e^{-\gamma_3 T}) . \tag{3.18}$$

It is now possible to rewrite (3.15) as

$$[\tilde{\rho}_{12}(t)]_n=E_{13}(t)\left[(1-\alpha)^{n-1}e^{-(n-1)\gamma_3 T}+(1-e^{-\gamma_3 T})\sum_{l=0}^{n-2}(1-\alpha)^l e^{-l\gamma_3 T}\right] , \tag{3.19}$$

where in the small-area approximation (2.20),

$$\alpha=\tfrac{1}{4}\theta_1\theta_2 e^{-(i\Delta-1/T_2)\tau} . \tag{3.20}$$

In the limit $\gamma_3 T\to 0$ and $n\gamma_3 T\to 0$, (3.19) reduces to

$$\tilde{\rho}_{12}(t)_n=E_{13}(t)(1-\alpha)^{n-1} \tag{3.21a}$$
$$=\tfrac{1}{8}ni\theta_1\theta_2^2 e^{i\Delta(t-\tau)}e^{-(t+\tau)/T_2}e^{-(n-1)\gamma_3 T} . \tag{3.21b}$$

This expression resembles that of the two-level model (2.24) with the factor $n$ replacing $(2n-1)$, and thus at large $n$ the echo amplitude (3.21) is one-half that of (2.24). The reason is that in the three-level case the population transfers rapidly from level 2 to the bottleneck level 3, reducing the grating population difference of levels 1 and 2 to one-half that of the two-level model.

On the other hand, for delay times $T$ long compared to the bottleneck storage time, $\gamma_3 T\gg 1$, memory of the population grating is lost. In the limit $\gamma_3 T\to\infty$ and $n\gamma_3 T\to\infty$, (3.19) becomes

$$[\tilde{\rho}_{12}(t)]_n=E_{13}(t) , \tag{3.22}$$

and the echo is due to the last pulse sequence $n$ alone.

For the case of arbitrary $\gamma_3 T$, we consider (3.19) again using the small-area approximation and write

$$[\tilde{\rho}_{12}(t)]_n = \tfrac{1}{8} i\theta_1\theta_2^2 e^{i\Delta(t-\tau)} e^{-(t+\tau)/T_2} \times \left[ n e^{-(n-1)\gamma_3 T} + (1-e^{-\gamma_3 T}) \sum_{l=0}^{n-2} (1+l) e^{-l\gamma_3 T} \right] . \quad (3.23)$$

Since the sum in (3.23) can be expressed as the derivative of a geometric series,

$$\sum_{l=0}^{n-2} l e^{-al} = -\frac{\partial}{\partial a} \sum_{l=0}^{n-2} e^{-al} = -\frac{\partial}{\partial a} \left[ \frac{1-e^{-(n-1)a}}{1-e^{a}} \right] , \quad (3.24)$$

where $a = \gamma_3 T$, it follows that

$$\tilde{\rho}_{12}(t)_n = \tfrac{1}{8} i\theta_1\theta_2^2 e^{i\Delta(t-\tau)} e^{-(t+\tau)/T_2} \left[ \frac{1-e^{-n\gamma_3 T}}{1-e^{-\gamma_3 T}} \right] . \quad (3.25)$$

The function

$$F(n) = \frac{1-e^{-n\gamma_3 T}}{1-e^{-\gamma_3 T}}$$

has the limiting values

$$\lim_{\gamma_3 T \to 0} F(n) = n , \quad (3.26)$$

$$\lim_{\gamma_3 T \to \infty} F(n) = 1 , \quad (3.27)$$

where (3.26) exhibits growth with increasing $n$ in agreement with (3.21b) and (3.27) shows no growth as predicted by (3.22).

## IV. OBSERVATIONS AND CONCLUSIONS

Photon echoes were monitored in the impurity ion crystal 0.1 at. % $Pr^{3+}$:$YAlO_3$. The crystal was in the form of a platelet with dimensions $5\times5\times1.1$ mm$^3$ parallel to the crystal axes $a:b:c$ and was immersed in liquid helium at 1.6 K. The beam of an ultrastable cw ring dye laser, possessing a linewidth of 300 Hz rms short term, passed through an acousto-optic modulator driven by a train of radio-frequency pulses and then propagated with a focused diameter of 75 $\mu$m along the $c$ axis of the crystal before striking a $p$-$i$-$n$ diode photodetector.

The laser beam was tuned to 610.5 nm to resonantly excite the $Pr^{3+}$ transition $^3H_4(\Gamma_1) \leftrightarrow {}^1D_2(\Gamma_1)$ and had a power in the sample of 2.5 mW. When the modulator was driven by a 95-MHz radio-frequency pulse, the beam was deviated and passed through an opening in an aperture and then through the sample. Between pulses, the undeviated beam was blocked by the aperture. The pulse generator was programed to produce a repetitive three-pulse sequence of adjustable width, frequency, delay, and amplitude. The first two pulses of equal amplitude and of 95 MHz frequency generate the echo signal while the third (probe) pulse of reduced amplitude of 97 MHz frequency overlaps the echo pulse in time to produce a readily detected 2-MHz heterodyne beat echo signal. To lengthen the $Pr^{3+}$ dephasing time and to increase the echo amplitude, a static field of 500 G was applied parallel to the crystal $b$ axis.

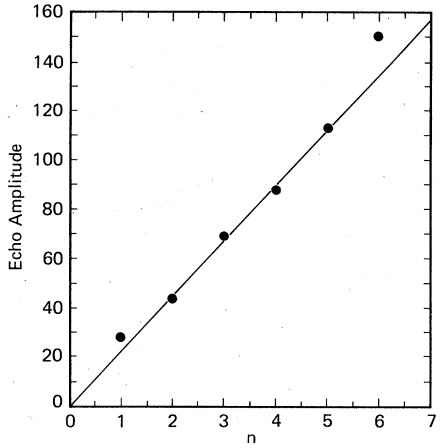


FIG. 4. Echo amplitude vs two-pulse sequence number $n$ showing near-linear behavior. The data are taken from Fig. 2.

The evolution of echo signals shown in Fig. 2 clearly reveals the growth behavior for a series of two-pulse sequences up to $n=6$, all applied pulses being activated by an electronic clock. Here, the pulse widths are $t_1 = t_2 = 2.5$ $\mu$sec, the pulse delay time $\tau = 6$ $\mu$sec, and the pulse sequence repetition time $T = 2$ msec. In Fig. 4, we see that the echo amplitude varies linearly with $n$ as predicted by (3.21b).

Due to the damping terms $e^{-n\gamma_3 T}$ and $e^{-\gamma_3 T}$ in (3.25), growth will begin to taper off when $n\gamma_3 T \sim 1$, and in principle this behavior would permit a measurement of $\gamma_3$, the decay rate of the bottleneck. For $Pr^{3+}$:$YAlO_3$, the bottleneck population decay must certainly be leakage among the $^3H_4$ hyperfine states with decay times exceeding one second. Attempts to see this saturation effect by lengthening $T$ failed because the modulator scatters $\sim 10^{-6}$ of the incident light through the aperture during the "dark periods," and the attendant optical pumping provides an additional path for erasing the population grating.

As a final comment, we emphasize that echo growth could not be observed in $Pr^{3+}$:$YAlO_3$ without using an ultrastable dye laser. If the laser frequency shifts from one pulse sequence to the next, the echo amplitude will not necessarily grow but may vary randomly as the laser samples new packets within the inhomogeneous line shape. Growth can occur only when the same packets are excited repeatedly. The problem is especially critical in impurity ion solids such as $Pr^{3+}$:$YAlO_3$ since the population grating spans a narrow frequency range of tens of kilohertz. Indeed, when the laser was not frequency and phase locked, the echo amplitude fluctuated wildly. It is clear that previous photon echo decay time measurements of these narrow line systems are subject to these amplitude fluctuations, which perhaps can be reduced to some extent by averaging.[12]

## ACKNOWLEDGMENT

This work was supported in part by the U.S. Office of Naval Research.

*On leave from the Physik Department, Universität Essen—Gesamthochschule, D-4300, Essen, West Germany.
[1]H. Y. Carr and E. M. Purcell, Phys. Rev. **94**, 630 (1954).
[2]I. Solomon, Phys. Rev. Lett. **2**, 30 (1959).
[3]S. Meiboom and D. Gill, Rev. Sci. Instrum. **29**, 688 (1958).
[4]J. S. Waugh, L. M. Huber, and U. Haeberlen, Phys. Rev. Lett. **20**, 180 (1968); E. D. Ostroff and J. D. Waugh, *ibid.* **16**, 1097 (1966).
[5]C. P. Slichter, *Principles of Magnetic Resonance* (Springer, New York, 1978), for additional discussion and references.
[6]J. Schmidt, P. R. Berman, and R. G. Brewer, Phys. Rev. Lett. **31**, 1103 (1973); P. R. Berman, J. M. Levy, and R. G. Brewer, Phys. Rev. A **11**, 1668 (1975).
[7]W. H. Hesselink and D. A. Wiersma, Phys. Rev. Lett. **43**, 1991 (1979); J. Chem. Phys. **75**, 4192 (1981).
[8]W. S. Warren and A. H. Zewail, J. Chem. Phys. **75**, 5956 (1981).
[9]J. B. W. Morsink and D. A. Wiersma, in *Laser Spectroscopy IV,* edited by H. Walther and K. W. Rothe (Springer, New York, 1979), p. 404.
[10]T. W. Mossberg, R. Kachru, S. R. Hartmann, and A. M. Flusberg, Phys. Rev. A **20**, 1976 (1979).
[11]R. G. Brewer, in *Frontiers in Laser Spectroscopy,* in Proceedings of the Les Houches Summer School, Session XXVII, edited by R. Balian, S. Haroche, and S. Liberman (North-Holland, Amsterdam, 1977), p. 341.
[12]F. Rohart and B. Macke, Appl. Phys. B **26**, 23 (1981).